Chapter 2

Principles of Microoptics and Portable LCDs

In this chapter, we describe the principle of diffractive microoptical components and portable LCDs. First, the diffraction angle and efficiencies of the two diffractive optical devices, Fresnel microlens and binary micro-grating, are discussed. Followed by characterizing the basic working principle of various portable LCDs, such as mixed-mode twisted nematic LCDs, super-twisted nematic LCDs, polymer dispersed liquid crystal, cholesteric LCDs, and double cell gap transflective LCDs. Finally, a briefly summary will be given.

2.1 Principle of microoptical components

Most classical macrooptical components, such as lens, prism, and mirror, are designed using the theory of geometrical optics, treating light as geometrical rays which will be refracted and reflected at optical interface, for example, between air and glass, as described by Snell's law. However, such structure is not easily fabricated in microstructure, especially in the dimensions of a few microns. Therefore, in the 70's and 80's, planner diffractive optical elements (DOEs) were developed. Diffractive optical elements have several advantages: 1. DOEs allow us to manipulate light fields in ways that would be unthinkable with traditional refractive and reflective optics; 2. DOEs can be cheap and light weight; 3. DOEs are more flexible in the design process.

To determine the optical path and efficiency of light transmitting in diffractive optical elements, scalar diffraction theory and vector diffraction theory are two main theories used in the design. Vector diffraction theory is a rigorous electromagnetic

theory, where light is treated as electromagnetic wave, and the propagation in optical system is derived by Maxwell equation. However, in most cases, the numerical computing is prohibitively time-consuming. In contrast, scalar diffraction theory is simple and efficient in calculation. However, scalar diffraction theory, derived from the Fourier optics, cannot deal with the phenomenon of polarization. In addition, scalar diffraction theory is only applicable for the large scale microstructure; namely, the variation of the surface-relief or index-modulation profile is larger than the wavelength of light λ, or the aspect ratio (depth/width) is similar to λ[24]. Fortunately, most microoptical elements are not so small in feature dimension, and the scalar diffraction theory is adequate to deal with most functions of DOEs[25], [26]. Therefore, the scalar diffraction theory are used on the designs in this thesis work.

2.1.1 Binary micro-gratings

Binary grating elements have the stepped approximation with respect to an ideal continuous phase profile. Diffraction efficiency of binary microoptical component depends on the number of steps in this staircase-like binary optical element. In typical VLSI lithography and etching process, the approximation to the desired thickness function is made to a set of 2^N discrete levels which are achieved by N mask lithography and etching (see chapter 3). Taking an example of blazed grating with constant spatial frequency, whose purpose is to deflect the incident light through a certain angle with the highest possible efficiency. Fig. 2-1 shows an ideal phase grating profile with a perfect sawtooth period, and a quantized version of that grating with 2^N level. The continuous blazed grating has the indication that 100% of incident light will be diffracted into a single first diffraction order if the peak-to-peak variation introduces exactly 2π radians. The binary optic approximation to grating is a quantized version with 2^N-levels. If there are 2^N steps of equal spaces and thickness existed in one period, one microprism in

grating, of this blazed phase grating, the thickness of the nth step is:

$$d_n = n \cdot d_1 = n \cdot \frac{\Delta_0}{2^N} \tag{2- 1}$$

Where Δ_0 is the peak-to-peak thickness of the blazed grating. If n_s denotes refraction index of the grating substrate, and λ denotes wavelength of light in air. The phase retardation of each step is expressed as:

$$\varphi_n = \frac{2\pi}{\lambda}[n_s - 1] \cdot d_n \tag{2- 2}$$

Thus, a normal incident light passing through the grating to induce phase change in the phase profile of each step is presented as:

$$\Psi(x, y) = \Psi_0 + \varphi_n \tag{2- 3}$$

The diffraction efficiency of this step approximation can be obtained by expanding its periodic amplitude transmission in a Fourier series. From these calculations, the diffraction efficiency of q-th diffraction order can be expressed by [27],

$$\eta_q = \sin c^2\left(\frac{q}{2^N}\right) \frac{\sin c^2\left(q - \frac{\Phi_0}{2\pi}\right)}{\sin c^2\left(\frac{q - \frac{\Phi_0}{2\pi}}{2^N}\right)} \tag{2- 4}$$

where Φ_0 is the peak-to-peak phase difference of this blazed grating, and is related to the peak-to-peak thickness variation through

$$\Phi_0 = \frac{2\pi(n_s - n_o)}{\lambda}\Delta_0 \qquad (2\text{- }5)$$

where n_0 is the refraction index of the surrounding.

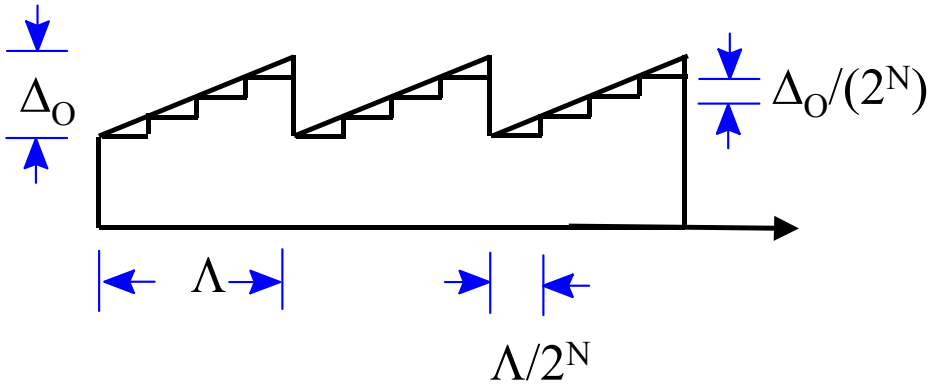

Fig. 2-1. Ideal sawtooh thickness profile for a blazed grating, and binary optical approximation to that profile.

Equation (2-4) is a general form of diffraction efficiency for a grating structure. Of special interest is the case of a quantized approximation to the blazed grating with a peak-to-peak phase difference of $\Phi_0=2\pi$, yielding

$$\eta_q = \sin c^2\left(\frac{q}{2^N}\right)\frac{\sin c^2(q-1)}{\sin c^2\left(\frac{q-1}{2^N}\right)} \qquad (2\text{- }6)$$

Therefore, diffraction efficiency of the primary order of interest, namely the +1 order (**q**=1), follows that:

$$\eta_1 = \sin c^2\left(\frac{1}{2^N}\right) \qquad (2\text{- }7)$$

The primary +1 order diffraction efficiency of the grating increases with the number of step (2^N).

Fig. 2-2 shows the diffraction spectra of gratings with N=2, 4, and 8 discrete phase levels. For N=2, the symmetry of the grating profile causes a symmetrical spectra with about 40.5% of the light being deflected into each of the two first orders. For N>2, the grating profile becomes asymmetrical; consequently, the spectrum becomes asymmetrical. The +1 order diffraction efficiency is 81% for a four-level grating and 95% for an eight-level grating.

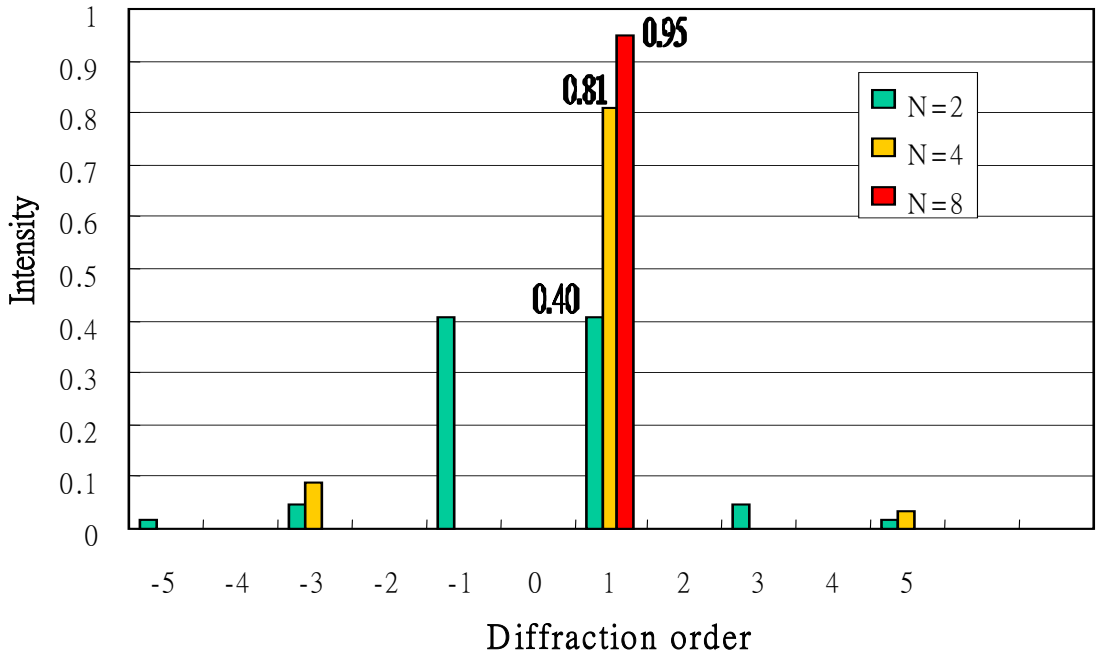

Fig. 2-2. The intensity in the diffraction orders for linear diffraction gratings with n phase levels.

Except diffraction efficiency, diffraction angle is another key factor shall be considered for designing a grating element. The grating element changes the optical wavefield and achieves desired optical functions by the periodic structure. The classical diffraction grating function can be taken to calculate the diffraction angle, as described by the grating equation,

$$\sin\theta_2 = \sin\theta_1 + m\lambda/\Lambda \quad . \text{(2- 8)}$$

where Λ is the period of grating, as illustrated in Fig. 2-1, m is the diffraction order. Obviously, the grating diffraction equation shows a direct relationship between structure's period and optical function.

2.1.2 Fresnel microlens

If the phase quantization procedure described above is applied to the circularly symmetrical phase profiles of microlens, it yields a set of annular rings which are typical for diffractive lenses. This annular ring structure is designed based on the Fresnel zone plate (FZPs) theory[28]. The ring system consists of continuous phase function or binary phase function structures to achieve whole phase diffraction elements. In both cases, the annular rings are designed such that the optical path lengths for the light deflected from adjacent zones towards a common focal point differ by an integral multiple of a design wavelength, as shown in Fig. 2-3. If r_i and f denote the radius of the i-th ring and the focal plane, respectively, this condition is expressed mathematically as[29][28]:

$$r_i^2 + f^2 = (f + i\lambda)^2 \quad \text{(2- 9)}$$

Thus, the radius r_i of the i-th zone follows that:

$$r_i^2 = 2i\lambda f + (i\lambda)^2 \quad \text{(2- 10)}$$

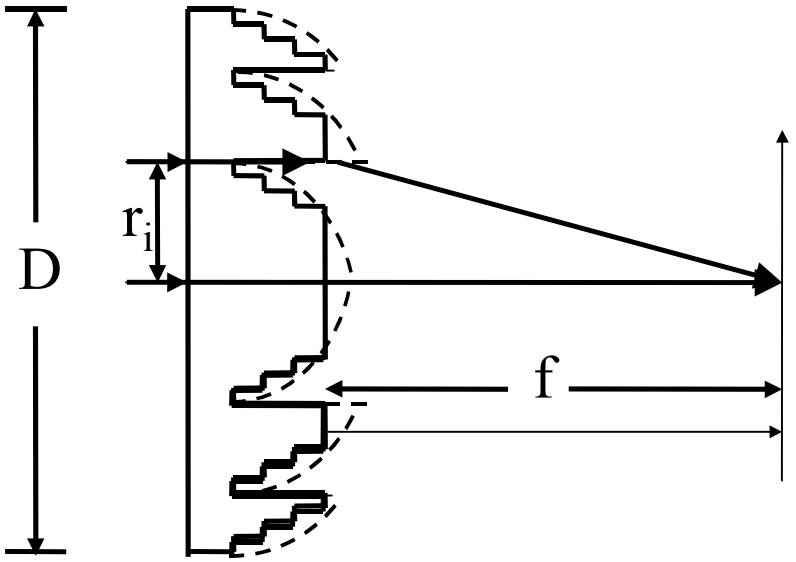

Fig. 2-3. Diffraction microlens of continuous and binary phase structure.

To meet this condition, the phase function $\Phi(x,y)$ of the binary Fresnel microlens is rewriten as:

$$\Phi(x,y)=\Phi(r^2)=\Phi\left(r^2+\mathrm{K}*r_p^{\,2}\right) \qquad (2\text{-}11)$$

where K is an integer, $r_p^{\,2}=2\lambda f$ is the period, and λ is the design wavelength. As $\Phi(x,y)$ is a periodic function, it can be expanded into Fourier series:

$$\Phi(r^2)=\sum_{m=-\infty}^{\infty}A_m e^{\left(j2m\pi\frac{r^2}{r_P^{\,2}}\right)} \qquad (2\text{-}12)$$

where A_m is the coefficient of Fourier series, namely the amplitude of each diffraction order:

$$A_m=\frac{1}{r_P^{\,2}}\int_0^{r_P^{\,2}}\Phi(r^2)e^{(-j2m\pi r^2)}dr^2 \qquad (2\text{-}13)$$

From the L –level quantized phase profile shown in Fig. 2-3, the phase function of this binary Fresnel lens is rewritten as

$$\Phi\left(r^2\right)=\sum_{k=0}^{N(L-1)}\exp\left(-\frac{j2\pi k}{L}\right)*rect\left(\frac{r^2-\frac{kr_p^{\,2}}{L}-\frac{r_p^{\,2}}{2L}}{\frac{r_p^{\,2}}{L}}\right) \tag{2- 14}$$

Substituting Eq. (2-15) into Eq. (2-13) yields the amplitude function as:

$$A_m=\sum_{k=0}^{N(L-1)}\exp\left(-\frac{j2\pi k}{L}\right)\int_{k/L}^{k+1/L}\exp(-j2\pi mx)dx \quad ; \quad \text{set} \quad x=\frac{r^2}{r_p^{\,2}}$$

$$=\sum_{k=0}^{N(L-1)}\exp\left(-\frac{j2\pi k}{L}\right)*\frac{1}{j2\pi m}*\exp\left(-j2\pi m\frac{k}{L}\right)\left[1-\exp\left(-j2\pi\frac{m}{L}\right)\right]$$

$$=\exp\left(-\frac{jm\pi}{L}\right)*\sin c\left(\frac{m}{L}\right)*\frac{1}{L}*\sum_{k=0}^{N(L-1)}\exp\left[-\frac{j2\pi k(1+m)}{L}\right] \tag{2- 15}$$

Observing Eq. 2- 15, we can get

$$\sum_{k=0}^{N(L-1)}\exp\left[-\frac{j2\pi k(1+m)}{L}\right]=\begin{cases}L\,,\,when\ m=I*L-1\,,\,I=\text{integer}\\0\ \,,\,others\end{cases} \tag{2- 16}$$

In order to enhance the intensity of focused light, this diffractive lens is optimized in certain diffraction orders. From the foregoing discussion, we use the –1 order diffraction to design the binary Fresnel lens. The diffraction efficiency is normalized by

$$\eta_{-1}=\frac{I_{-1}}{\sum_{m=-\infty}^{\infty}I_m}=\sin c^2\left(\frac{1}{L}\right) \tag{2- 17}$$

The diffraction efficiency of different levels binary lens can be directly calculated from Eq. (2-17). As shown in Fig. 2-4, high diffraction efficiency can be achieved with more levels approximation. We obtain similar diffraction efficiency equations of diffractive grating Eq. (2-7) and diffractive lens Eq. (2-17). Exactly, the diffractive lens structure can be considered as an annular grating with varying periods for reflected light focusing. In the central part of lens, the grating periods are larger, therefore, the quantization of the phase profile into more levels (>8) is simple and not critical. However, the grating periods become smaller towards the rim. The number of the phase levels is limited by the resolution of fabrication process, such as VLSI lithography. This limitation in fabrication also restricts the F-number of diffractive lens as:

$$\Delta R_{\min} = R_m - R_{m-1} = \frac{\lambda}{2} \cdot \frac{f}{D} = \frac{\lambda}{2} \cdot (F/\#) \qquad (2\text{- }18)$$

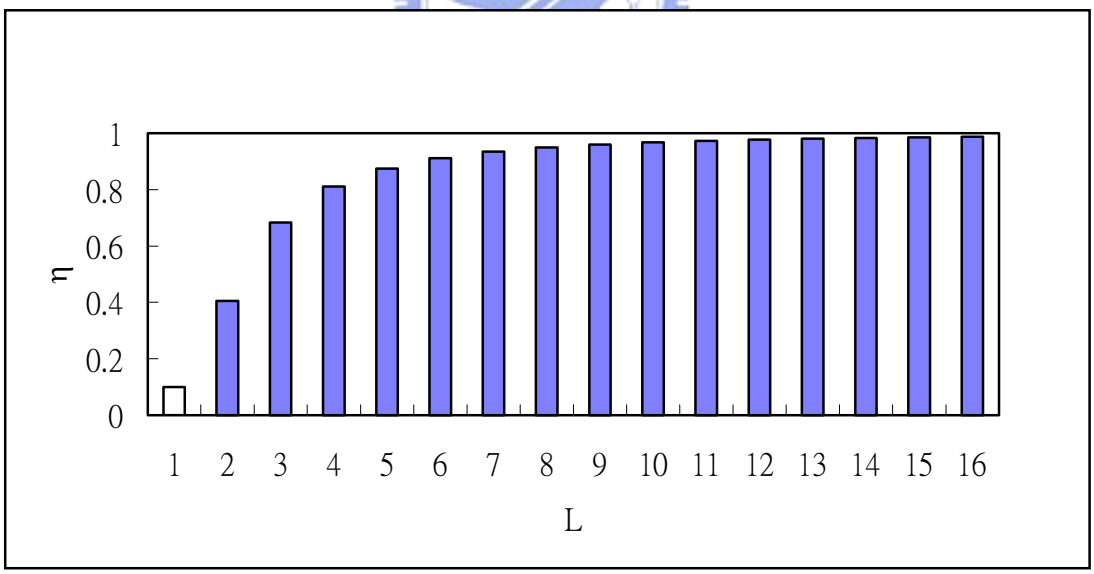

Fig. 2-4. Efficiencies of diffractive lens at focal point vs. the number of phase levels[29]. Here N=1 refers to an amplitude of Fresnel zone plate.

2.2 Principle of portable LCD technologies

Reflective LCDs utilizes ambient light to read out the displayed images. Low power consumption and light weight are its advantages, thus are much suitable for handheld and outdoor applications. The reflective LCDs can be roughly categorized into two types: single and non polarizer. The single-polarizer type, such as mixed-mode twisted nematic LCDs (MTN-LCDs) and super-twisted nematic LCDs (STN-LCDs), have lower reflectivity due to the linear polarizer only has 45% transmittance for unpolarized incident light. However, they exhibit a better contrast ratio than a non-polorizer LCD. The single-polarizer LCD offers a compromise between display brightness and contrast ratio, and has gradually become the mainstream approach. Contrary, the LCD that does not require polarizer, such as polymer dispersed liquid crystal (PDLC) and cholesteric LCDs (Ch-LCDs), has the advantage of higher reflectivity and wider viewing angle yet with lower contrast and poor color image. Consequently, in some applications where high brightness is more critical than contrast ratio, these LCDs are more attractive.

2.2.1 Mixed-mode twisted nematic LCDs (MTN-LCDs)

The MTN cell has been shown to exhibit a high contrast ratio, low voltage, and weak color dispersion under the single polarizer configuration[30].A typical MTN reflective display consists of a polarizer, ideal λ/4 retardation film, and a twisted LC cell with a reflector embedded on the inner side of the rear substrate[31]. The incident light traverses the linear polarizer, λ/4 film and LC layer, and is reflected back by the embedded mirror in the inner side of the rear substrate, as shown in Fig. 2-5. Under the crossed-polarizer configuration, to obtain high refelctance in the voltage-off state the LC cell needs to function as an achromatic λ/4 plate. Therefore, the incoming

linearly polarized light passes the two cascaded λ/4 plate twice upon reflection and is transmitted by the polarizer.

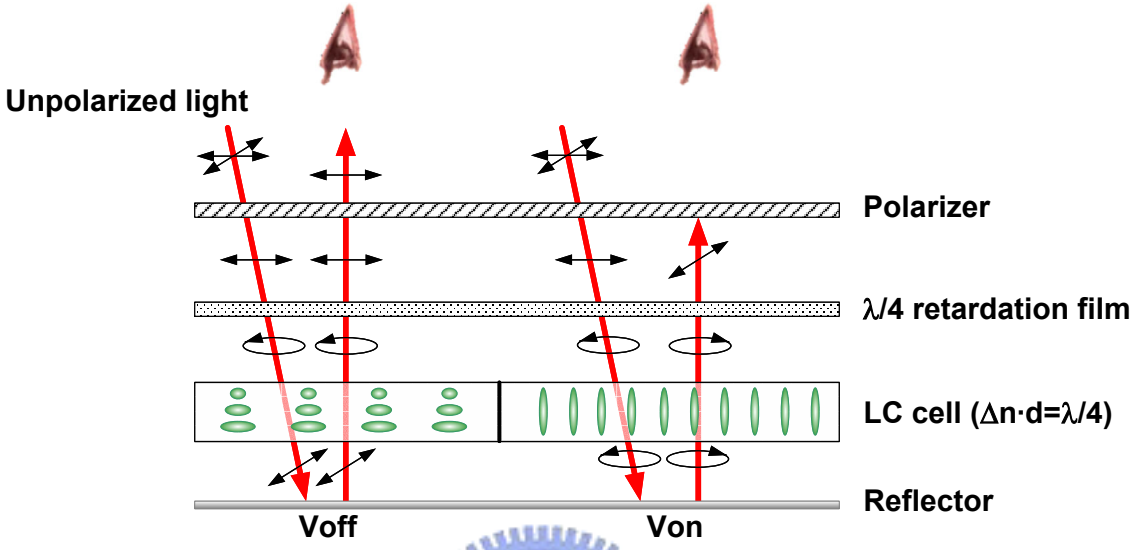

Fig. 2-5. Schematic plot of the basic working principle of MTN LCD.

The output of an optical system can be determined by considering the transmission of a plane wave with an arbitrary polarization through an optical system which maintains the plane-wave nature of the wave but alters its polarization. Under the above-mentioned reflective display configuration, the Jones matrix[32], [33], [34] is used to calculate the reflectance of a MTN-LCD. Fig. 2-6 illustrates schematically the optical system with all the parameters determining polarization of a reflective LC module. For the scale of simplicity, the transmittance axis of the polarizer is taken to be the horizontal direction. The angle between the polarizer and the λ/4-wave plate is 45°. The top LC director is at an angle β with respect to the axis of the polarizer, and ϕ_{LC} is the twist angle of an LC cell. Under the above-mentioned reflective display configuration, the optical reflectance($R_{\perp}$) of a MTN-LCD can be described by $|\boldsymbol{M}|^2$ [30] with:

$$M = \left|\cos\beta \quad \sin\beta\right| \begin{vmatrix} \cos X - i\frac{\Gamma}{2}\frac{\sin X}{X} & -\phi_{LC}\frac{\sin X}{X} \\ \phi_{LC}\frac{\sin X}{X} & \cos X + i\frac{\Gamma}{2}\frac{\sin X}{X} \end{vmatrix} \times \begin{vmatrix} \cos X - i\frac{\Gamma}{2}\frac{\sin X}{X} & \phi_{LC}\frac{\sin X}{X} \\ -\phi_{LC}\frac{\sin X}{X} & \cos X + i\frac{\Gamma}{2}\frac{\sin X}{X} \end{vmatrix} \begin{vmatrix} -\sin\beta \\ \cos\beta \end{vmatrix} \quad (2\text{- }19)$$

Here β is the angle between the polarization axis and the front LC director, ϕ_{LC} is the twist angle, $X = \sqrt{\phi_{LC}^{\,2} + (\Gamma/2)^2}$ and $\Gamma = 2\pi d\Delta n / \lambda$, where d is the cell gap.

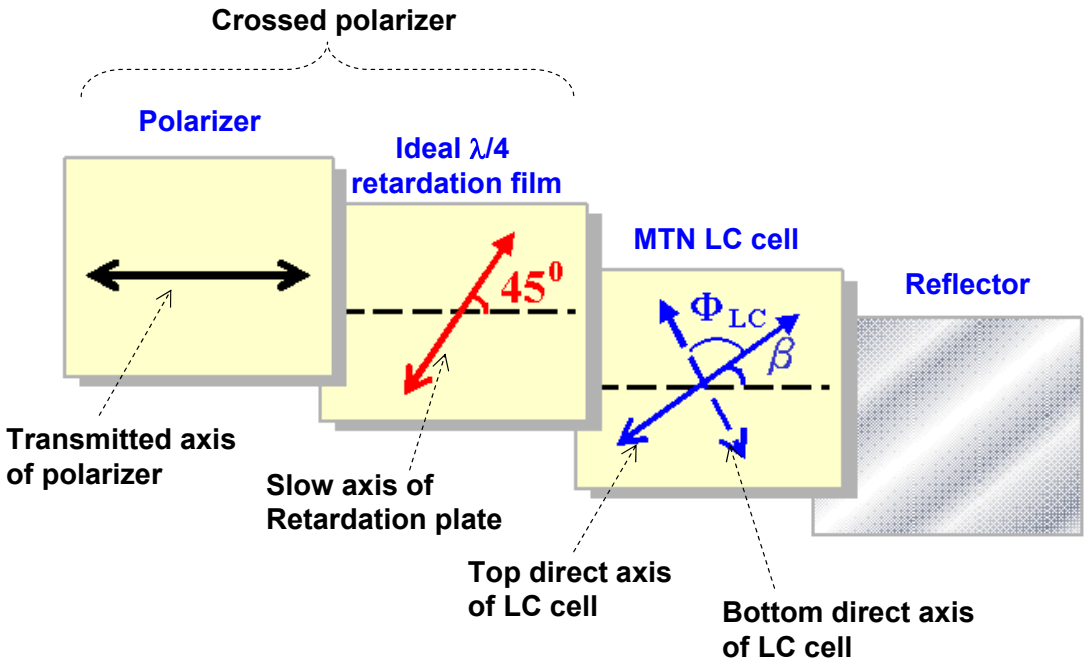

Fig. 2-6. The parameters of a general MTN display employing polarizer, retardation film and reflector.

To illustrate the design principles, we use Eq. 2- 19 to plot the normalized reflectance ($R_\perp$) as a function of $d\Delta n/\lambda$ and β for 90° MTN cell. Fig. 2-7 depicts the simulation results of $R_\perp$ at $\beta = 0°$, 20°, and 40°[35]. At $\beta = 0°$, the peak reflectance only reaches about 70%. As β increase to 20°, the maximum reflectance ($R_\perp = 88\%$) occurs at $d\Delta n/\lambda \cong 0.45$. As β continues to increase, the maximum reflectance gradually

declines. Therefore, for a MTN cell with $\phi_{LC} = 90^o$, $\beta = 20^o$ can provides highest reflectance.

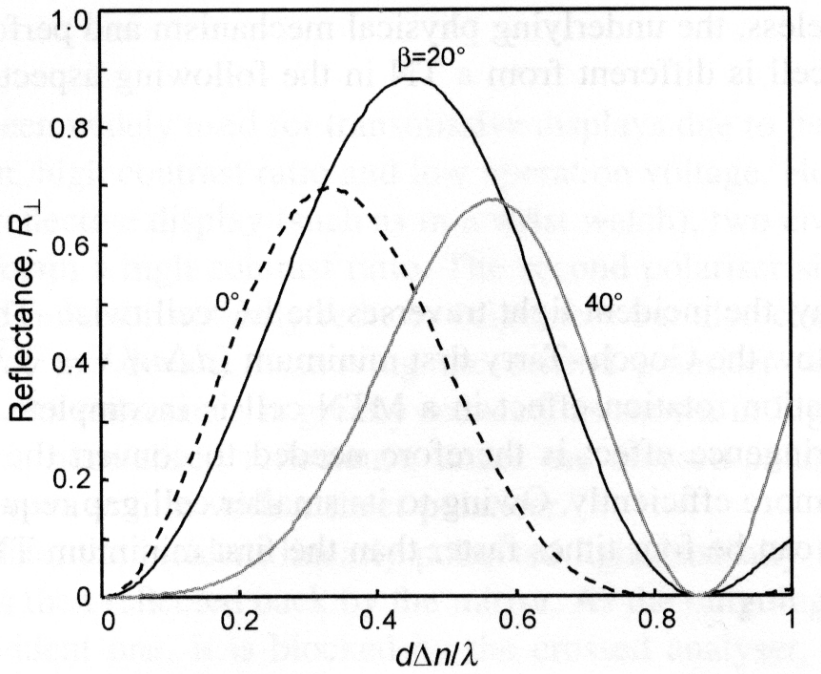

Fig. 2-7. Simulated results of the normalized reflectance $R_\perp$ of a 90° MTN cell as a function of $d\Delta n/\lambda$ and β.

The LC director distributions and corresponding electro-optic (E-O) properties of the LC cell can be calculated by using Oseen-Frank elastic continuum theory[36], [37] and extended Jones matrix method[38], respectively. Additionally, several commercial simulation packages, such as DiMos[39] and LCD Master[40], are available to calculate the E-O curves of LC cell. The calculated results of the voltage-dependent reflectance of 90° MTN cell with $d\Delta n$=240nm and $\beta = 20^o$ are shown in Fig. 2-8. In the voltage-off state, the RGB colors show high reflectance with similar value, thus the image appears white. At 5 V_{rms}, a good common dark state is obtained for the three colors. A calculated contrast ratio of 300 : 1 can be yield without considering the influence of surface reflection. In the real case, however, the surface reflection decreases the contrast ratio to only around 15 : 1.

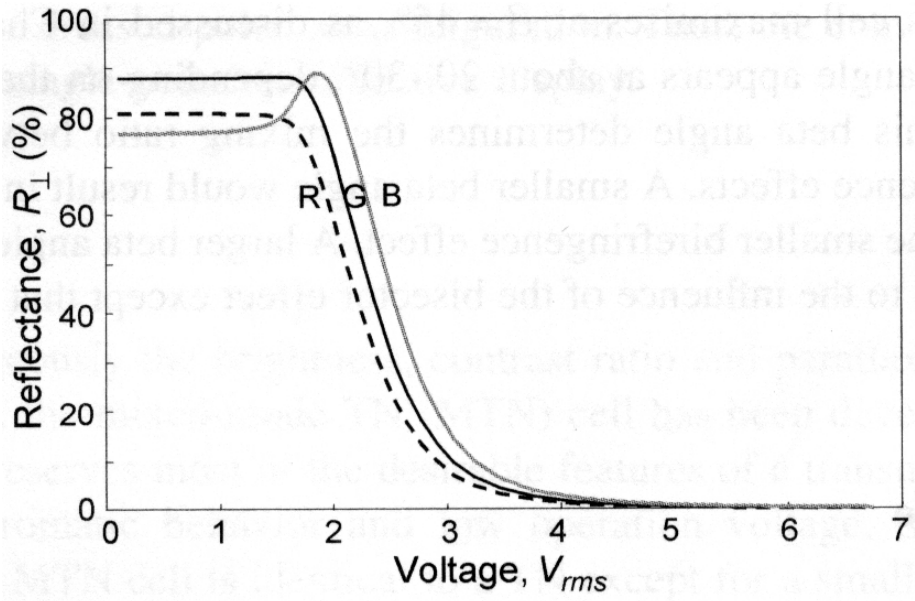

Fig. 2-8. Normalized reflectance $R_\perp$ of R, G, and B colors of a 90° MTN cell ($d\Delta n$ = 240nm and β=20°) used in a single-polarizer reflective display.

2.2.2 Super-twisted nematic LCDs (STN-LCDs)

A super-twisted nematic (STN) cell is defined as one in which the LC twist angle is greater than 90°. In order to make the twist angle larger than 90°, a small percentage of chiral agent needs to be doped into the LC mixture. A STN display is know to exhibit a much steeper electro-optic curve than MTN display so that the simple low-cost passive matrix addressing method[41] can be applied. From the Alt-Pleshko theory of multiplexing[42], the number of multiplexing lines (N) is determined by the selection ratio of the on- and off-state voltages as

$$\frac{V_{on}}{V_{off}} = \left(\frac{\sqrt{N}+1}{\sqrt{N}-1} \right)^{1/2} \qquad (2\text{-}20)$$

A graph of Eq. (2- 20) is shown in Fig. 2-9 for convenience. In order to have N > 200 for a high-information content STN display, the voltage selection ratio should be of less than 1.073.

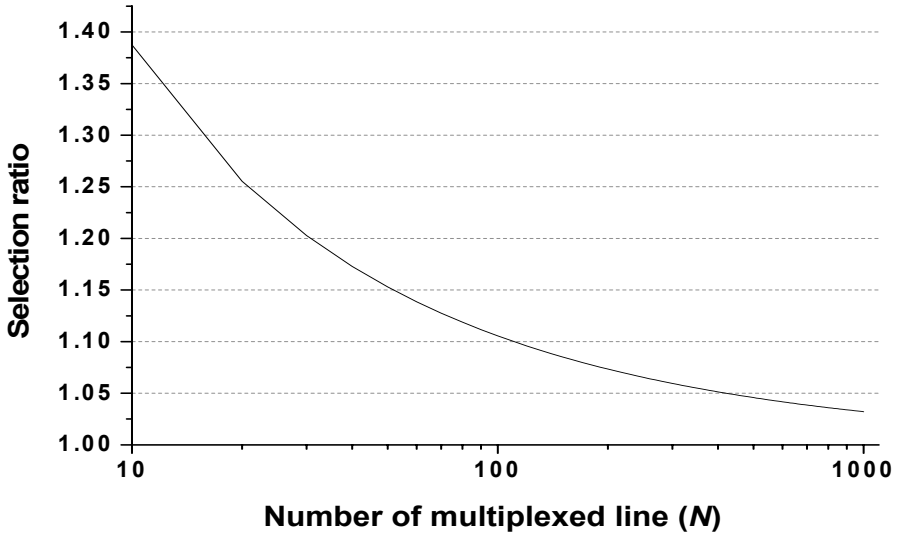

Fig. 2-9. The relationship between voltage selection ratio and multiplexing line.

The basic working principle of STN-LCD is quite similar to that of MTN-LCD. The only difference is that the LC twist angle ϕ_{LC} of STN is larger than 90°. A general configuration of reflective STN display is depicted in Fig. 2-10. The normalized reflectance ($R_\perp$) of such a STN cell can also be calculated by the Jones matrix method:

$$R_\perp = \left(\Gamma \frac{\sin X}{X}\right)^2 \left(\sin 2\beta \cos X - \frac{\phi}{X} \cos 2\beta \sin X\right)^2 \qquad (2\text{-}21)$$

Here $\Gamma = 2\pi d\Delta n / \lambda$, d is the LC cell gap, $X = \sqrt{{\phi_{LC}}^2 + (\Gamma/2)^2}$ and ϕ_{LC} is the twist angle. β is the angle between the polarization axis and the front LC director. Using Eq. 2- 21, one should be able to find the optimal cell parameters (e. g. dΔn and β) for a given twist cell and then calculate its voltage-dependent reflectance.

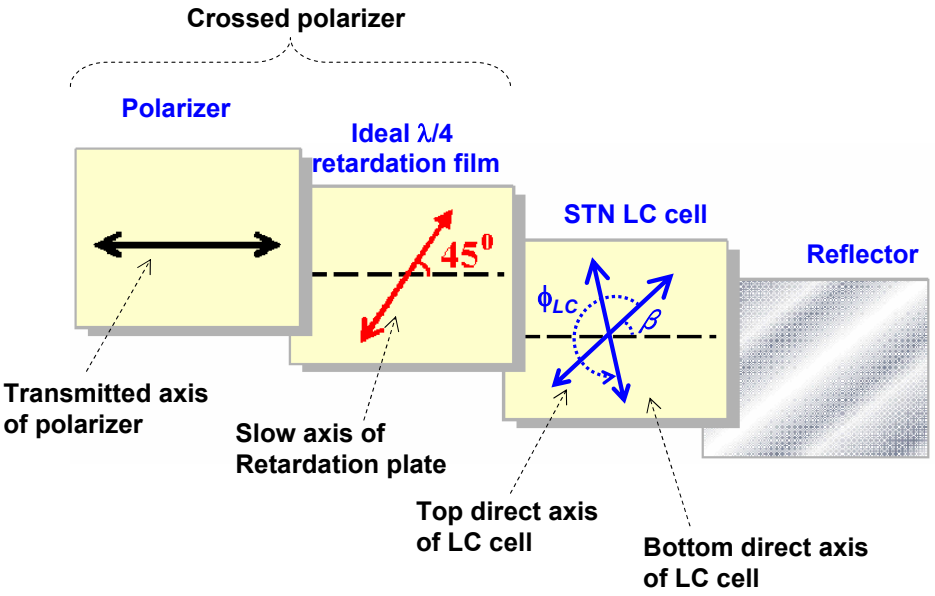

Fig. 2-10. The parameters of a general STN display employing polarizer, retardation film and reflector.

Take a ϕ_{LC} = 210° STN cell as an example, eq. 2- 21 is used to obtain optimal cell parameters. The $d\Delta n/\lambda$ dependent normalized reflectance at β = -10°, 0°, 10° and 20° is shown in Fig. 2-11. The maximum reflectance that can be obtained is 96% which occurs at β = 10° and $d\Delta n \cong 1.14\lambda$.

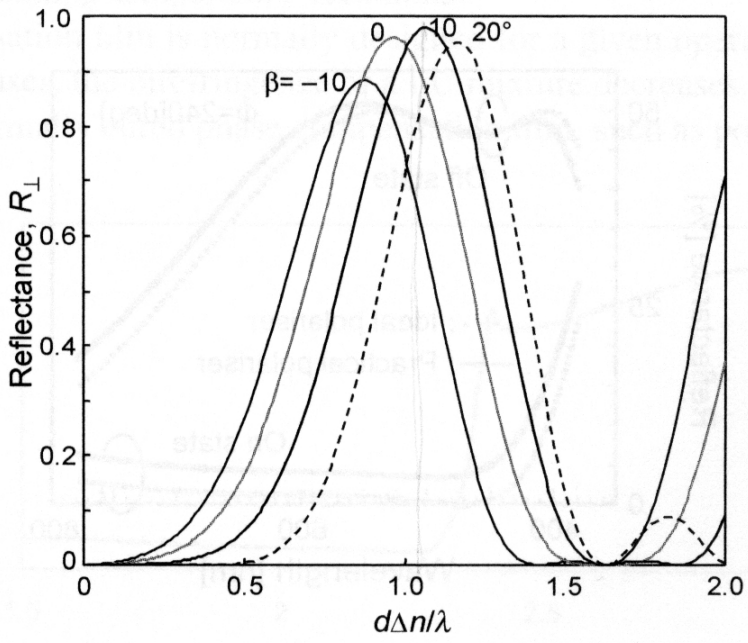

Fig. 2-11. Simulated results of the normalized reflectance $R_\perp$ of a 210° STN cell as a function of $d\Delta n/\lambda$ and β.

From the optimized design of Fig. 2-11, $d\Delta n$ = 630nm, β = 10° are used to simulate the voltage-dependent reflectance of the 210° STN cell for the R, G, and B three primary colors, as shown in Fig. 2-12. For the Voltage-off state, the highest reflectivity occurs at green wavelength. In this case, both blue and red have much lower reflectance in the voltage-off state. As voltage increases, $R_\perp$ decreases monotonically and display dark image occurs at 2.50 V_{rms}. Obviously, the dispersion of 210° STN cell (Fig. 2-12) is much serious than that of 90° MTN cell (Fig. 2-8). Therefore, a double retardation films approach was proposed to reduce the color dispersion[43], where the results shown in Fig. 2-13. Consequently, a reflective color-STN LCD with VGA resolution, 4096 colors, 1/240 duty ratio, 15% reflectance, 14:1 contrast ratio, 250 ms response time and 89 mW power consumption has been demonstrated[44].

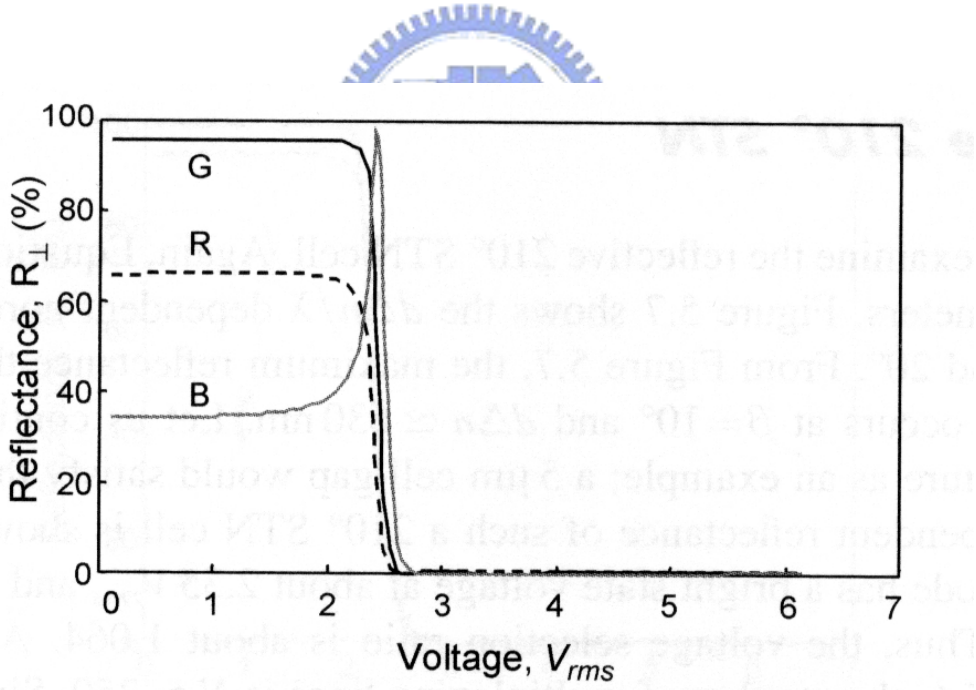

Fig. 2-12. Normalized reflectance $R_\perp$ of R, G, and B colors of a 210° STN cell (dΔn = 630nm and β=10°) used in a single-polarizer reflective display.

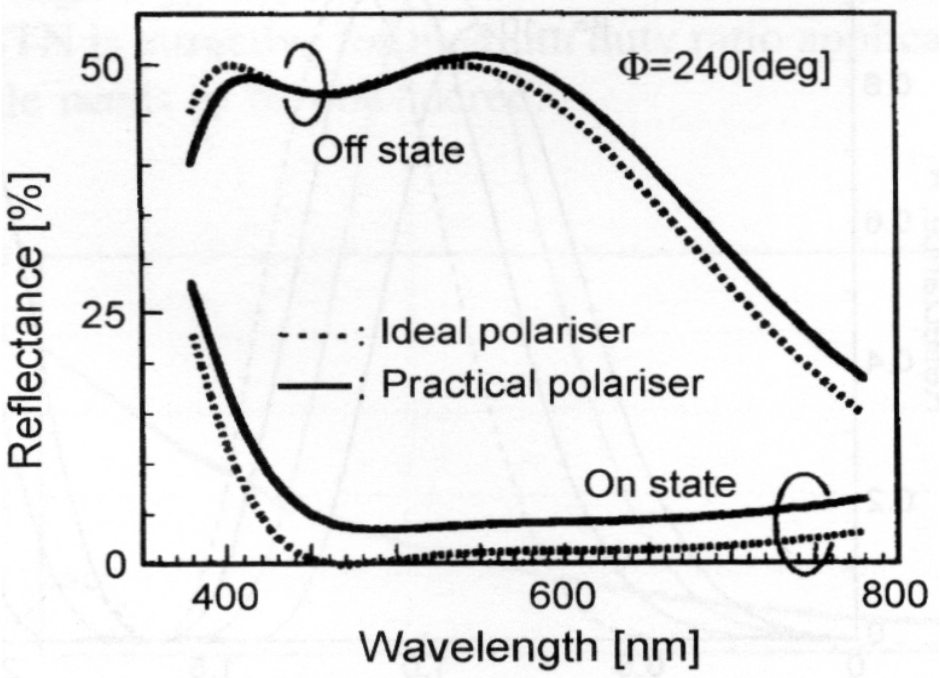

Fig. 2-13. The wavelength-dependent light reflectance of reflective color-STN cell with double retardation film.

2.2.3 Polymer dispersed liquid crystal (PDLC)

Polymer dispersed liquid crystal (PDLC) technology are relatively new class of materials which have been used in displays[45]. It has the advantage over regular LCDs in that it does not need polarizers and therefore the transmittance or reflectance is very high in the transparent state. It is suitable for use in applications where high transmittance is required. Its compatibility with plastic substrates is another advantage, because the non-uniform birefringence of plastic substrates does not cause problems. For PDLCs, the polymer binder is self-adhesaive, making it possible to fabricate large displays using a roll-to roll process.

PDLC consist of low molecular weight liquid crystals and polymers, and the liquid crystals are confined in droplets. The operation principle of a PDLC is based on light scattering induced by the refractive index mismatch between micron-sized LC droplets and the surrounding polymer matrices[46], as presented in Fig. 2-14. When a

PDLC is in the field-off state, the orientation of the droplets is random through the sample; the incident light encounters different refractive indices in the polymer binder and the liquid crystal droplets, and therefore it is scattered. When the PDLC is in the field-on state, the droplets are aligned in the cell normal direction; the incident light is transmitted.

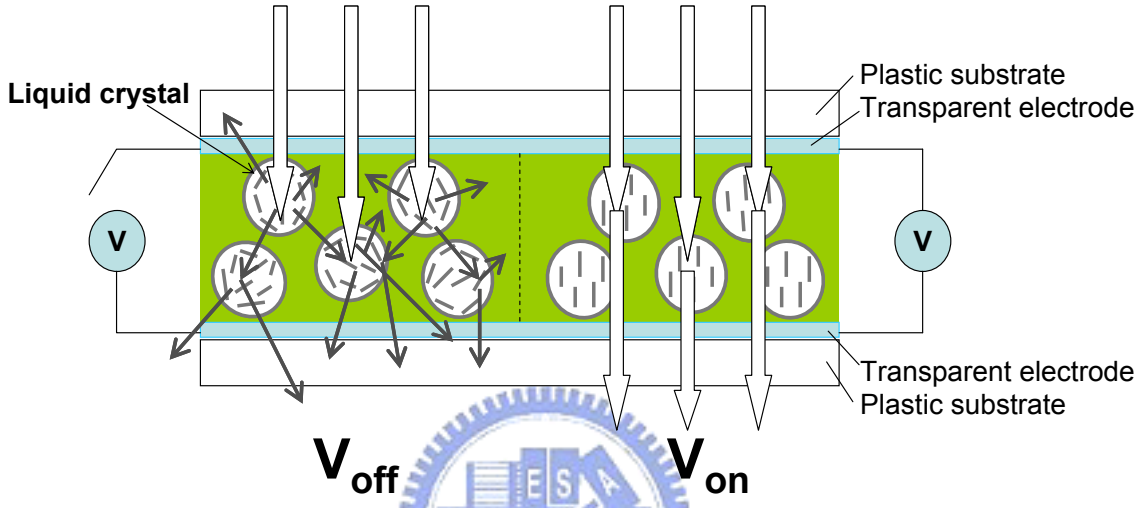

Fig. 2-14. Orientation of liquid crystal droplets in the off and on states in the PDLC.

In reflective PDLC displays, dichroic dyes are incorporated into PDLCs[47]. The black dye molecules are usually elongated and can be dissolved in the liquid crystal. The dye and liquid crystal phase separate from the polymer binder. They are inside the droplet and can be switched. When the polarization of the incident light is parallel to the long axis of the dye molecules, the light is absorbed[48]. When the polarization of the incident light is perpendicular to the long axis of the dye molecules, the light is not absorbed. In the field-off state, the dye molecules are randomly oriented with the droplets, as shown in the left part of Fig. 2-15. When the cell is sufficiently thick, there are droplets oriented in every direction. The unpolarized incident light is absorbed. In the field-on state, the dye molecules are aligned in the cell normal direction with liquid crystal, as shown in the right part of Fig. 2-15. The dye are

always perpendicular to the polarization of normally incident light. Therefore the light ideally passes through the cell without absorption. The typical voltage-absorbance curve of a dye doped PDLC is shown in Fig. 2-16 [49], as applied voltage is increased, the droplets become more and more aligned in the cell normal direction, and the absorbance decreases. The maximum transmittance is about 70%, which is lower than that of pure liquid crystal PDLC, due to the non-perfect order of dye molecules.

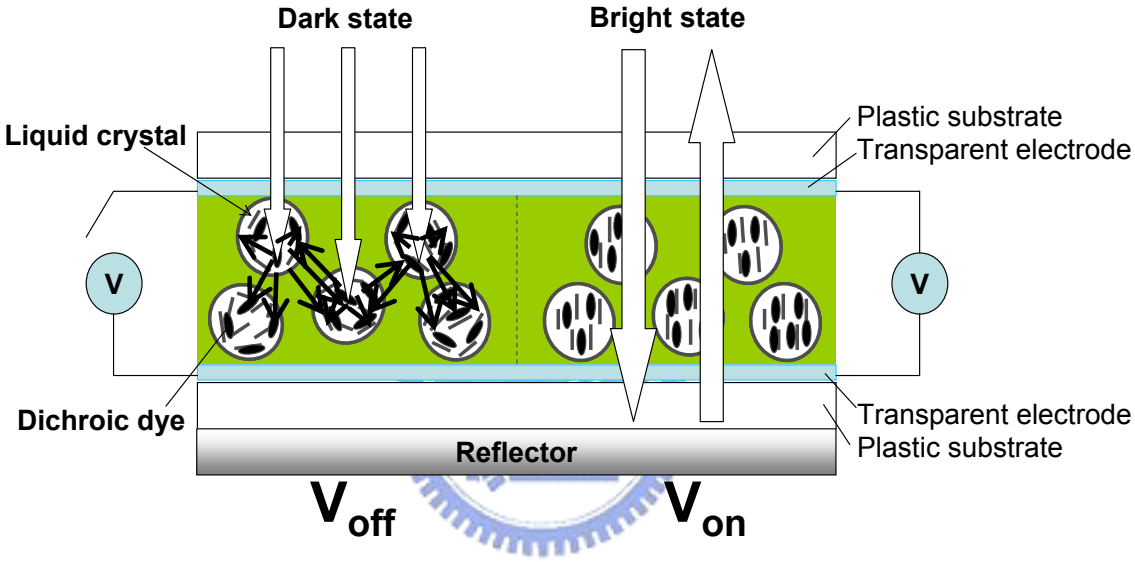

Fig. 2-15. Schematic diagram showing the working principle of reflective PDLCs.

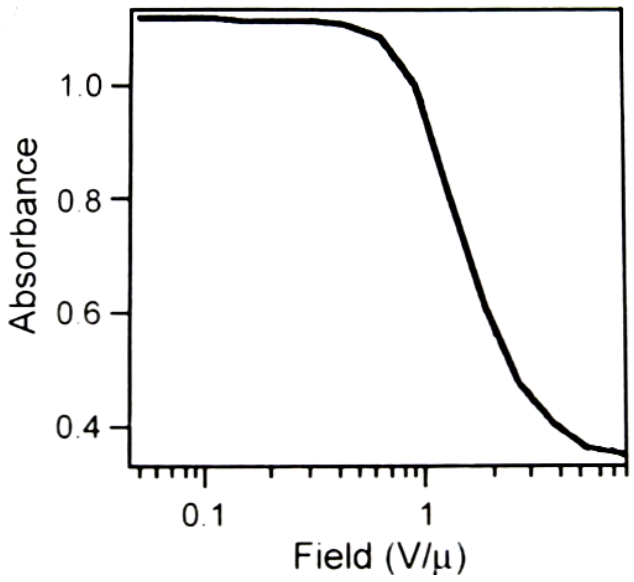

Fig. 2-16. Absorbance of the dye doped PDLC versus the applied field[49].

The typical reflection spectra of a dichroic dye doped PDLC are shown in Fig. 2-17[50]. The averaged reflectance of the field-on state is around 65% and the contrast ratio is 8 : 1.

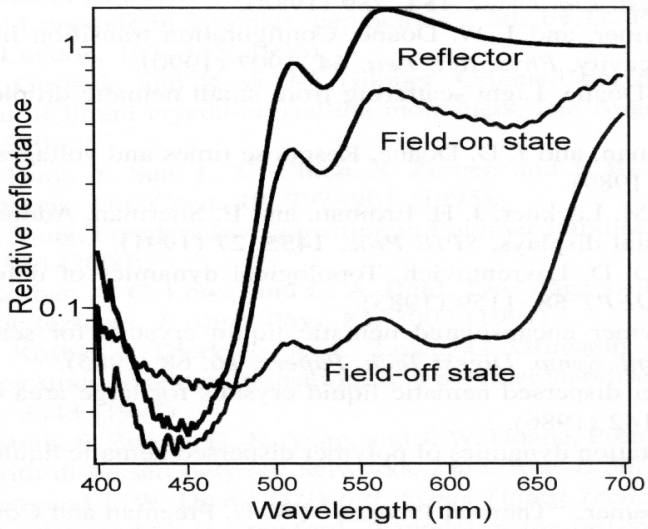

Fig. 2-17. Reflection spectra of the reflector and the dichroic dye doped PDLC reflective display[50].

There are a few points worth emphasizing for reflective PDLC displays. First, in the field-off state the scattering of the material increases the optical path length of the light inside the cell, and therefore enhances the absorption. Second, dye doped PDLC do not need polarizers, because of random orientation of the droplets in the field-off state can absorb most of the incident light, which is an advantage over conventional LCDs. Third, dye doped PDLCs have gray levels, because the droplets are gradually aligned by increasing the applied field. Fourth, the reflectance of the field-on state is high, yet the contrast is only acceptable. Fifth, it is compatible with plastic fabrication process, which is easily fabricated and low cost.

2.2.4 Cholesteric LCDs (Ch-LCDs)

The cholesteric (Ch) phase is a liquid crystal phase exhibited by chiral molecules or mixtures containing chiral components. The state of the cholesteric liquid crystal is

characterized by the direction of the helical axis as shown in Fig. 2-18[51]. In the planar texture, the helical axis is perpendicular to the cell surface as shown in Fig. 2-18(a). The material reflects light centered at wavelength given by $\lambda_0=nP_0$, where n is the average refractive index. If λ_0 is in the visible light region, the cell has a bright colored appearance. In the focal conic texture, the helical axis is more or less parallel to the cell surface, as shown in Fig. 2-18(b). When the pitch is short, the cholesteric liquid crystal can be regarded as a layered structure, which is a multiple domain structure, and the material is scattering. When the applied field is larger than a critical field *Ec*, the helical structure is unwound with the liquid crystal director aligned in the cell normal direction as shown in Fig. 2-18(c). This texture is called the homeotropic texture. With the appropriate surface anchoring condition or dispersed polymer, both the planar texture and the focal conic texture can be stable at zero field.

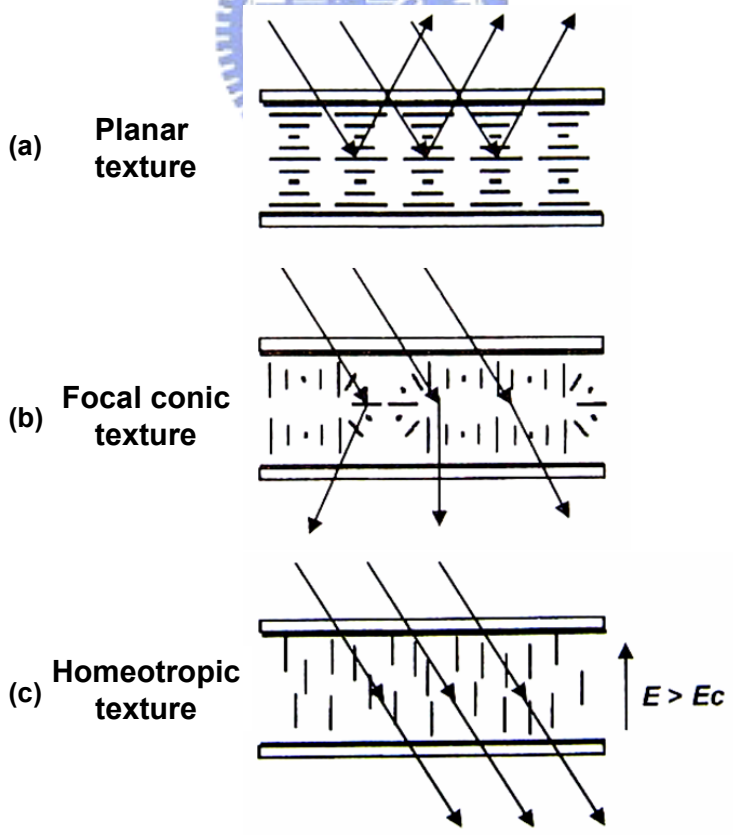

Fig. 2-18. The structure of the cholesteric textures: (a) planar, (b) focal conic, and (c) homeotropic texture.

The operation principles of Ch-LCDs are illustrated in Fig. 2-19. In the voltage-off state, the planar texture reflects brilliant colored light if the Bragg reflection condition ($\lambda_0=nP_0$) is satisfied[52], [53]. The bandwidth $\Delta\lambda$ of the reflected light is equal to ΔnP_0; here Δn is the birefringence of the LC. For a display in the visible region, $\lambda_0 \approx 550$nm, n ≈ 1.6 and $\Delta n \approx 0.2$, the pitch length P_0 is 344nm and the bandwidth $\Delta\lambda$ is 70nm. In a helical structure, circularly polarized light with the same handedness as the helical structure is reflected strongly because of constructive interference of the reflected. While circularly polarized light with the opposite handedness to the helical structure is not reflected because of the destructive interference. For an incident unpolarized light is decomposed into right and left circular polarized components with one component reflected and the other transmitted. The transmitted light is absorbed by the black paint coated over the rear substrate, as shown Fig. 2-19(a). In a voltage-on state (Fig. 2-19(b))[54], the periodic helical structures are changed to focal conic. As a result, the Bragg reflection is interrupted. The incoming light is absorbed by the dark paint and a dark state is obtained.

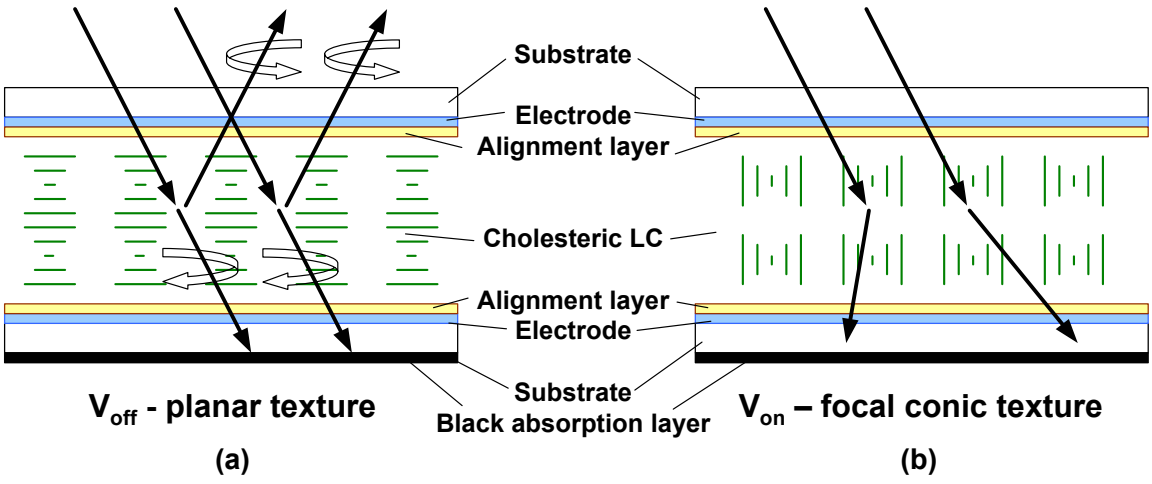

Fig. 2-19. The basic operation principle of a reflective cholesteric LCD at (a) Voltage-off and (b) Voltage-on state.

Although cholesteric liquid crystals are only bi-stable, they exhibit gray scale memory states because of their multi-domain structure[55],[56]. Starting from the imperfect planar texture, some domains can be switched to the focal conic texture at lower voltages than other domains. Once a domain has been switched to the focal conic texture, it remains there even after the applied voltage is turned off. Fig. 2-20 shows microphotographs of the gray scale states of a cholesteric display. From right to left, the states are achieved by applying voltage pulses with increasing amplitude, and the reflectance decreases. The domain size is around 10 μm and the domain structure cannot be observed by the naked eye. The typical pixel size for Ch-LCD is about 200μm. It is misleading to call the Ch-LCD multi-stable. A cholesteric domain has only two stable states at zero field: it is either in the planar texture or in the focal conic texture. In a Ch-LCD, it is observed that the domains in the planar texture have the same optical properties, independent of the states of other domains.

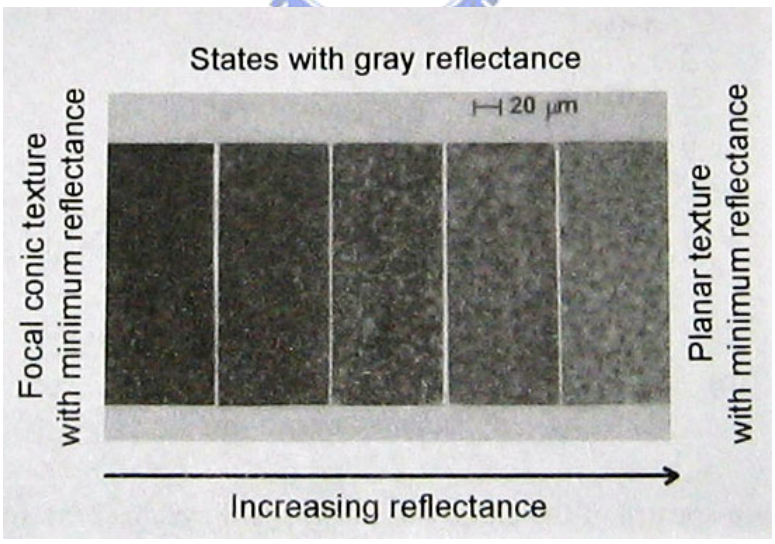

Fig. 2-20. The microphotographs of the gray scale states of the cholesteric display[17].

An important advantage of the Ch-LCD is that the reflected light is already colored. Therefore, a mono-color display without using color filters can be easily

achieved. In addition, no polarizer is needed. Thus, the brightness of a Ch-LCD is higher than a reflective color display employing one polarizer. To achieve multiple colors, three monochrome R, G, and B panels can be stacked together[57], [58]. A potential problem of the stacked approach is parallax, i.e. the incident light and reflected light pass through different pixels. Parallax leads to color mixing which becomes a serious issue for high-resolution LCD. In order to decrease parallax, thin substrate, preferably substrates with conducting coating on both sides, should be used to decrease the spacing between the liquid crystal layers. The measured reflection spectra of three-layer cholesteric display is shown in Fig. 2-21[58]. Without using a polarizer, the reflectance is around 30% ~ 35%, and its contrast ratio is in the range of 5-10 within 60° viewing cone.

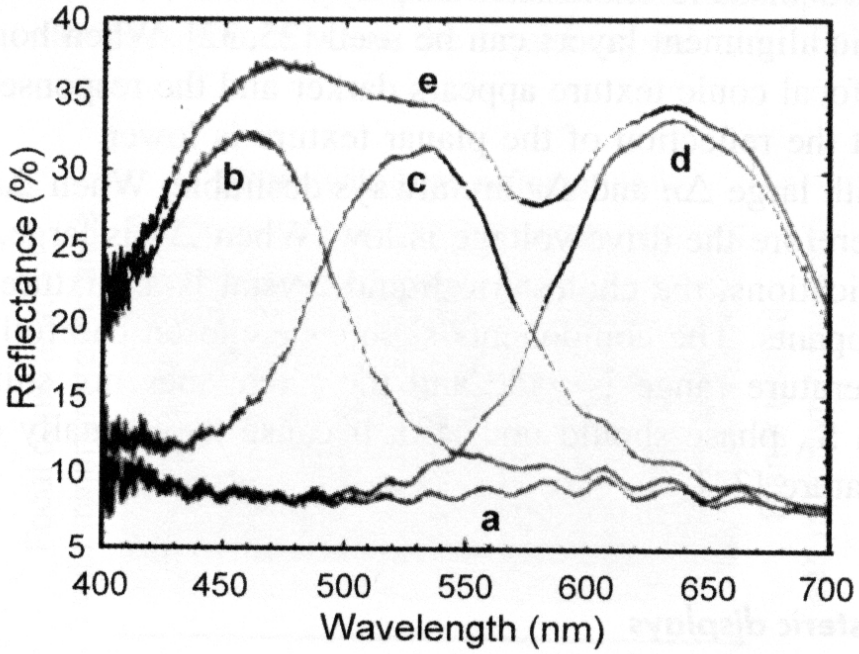

Fig. 2-21. Reflection spectra of the stacked multiple color cholesteric display. Curve a: all off, curve b: blue on, curve c: green on, curve d: red on, curve e: all on[58].

However, the stacking method is still too complex to fabricate a full color Ch-LCD. Additionally, conventional cholesteric LCD cannot display same image

color in reflective and transmissive modes. Therefore, it cannot be used in different ambiences, thus, restricting the applications of Ch-LCDs.

2.2.5 Transflective LCDs (TR-LCDs)

We had briefly introduced the basic working principle of single and double cell gap transflective LCDs in chapter 1. Hence, only the simple numerical formulas for explaining the LC optical efficiency are derived below.

When a plane wave is incident normally to uniaxial liquid crystal layer sandwiched between two polarizers, the outgoing will experience a phase retardation δ due to the different propagation velocities of the extraordinary and ordinary rays inside the LC [59] as shown in Eq. 2- 22:

$$\delta = \frac{2\pi d}{\lambda}(n_e - n_o) = 2\pi d\Delta n / \lambda \qquad (2\text{-}22)$$

Where d is the cell gap, Δn is the birefringence and λ is the wavelength. When a normally white homogeneous cell is sandwiched between two polarizers, the normalized light transmittance is governed by Eq. 2- 23:

$$T = \cos^2\chi - \sin 2\beta \sin 2(\beta - \chi)\sin^2(\delta/2) \qquad (2\text{-}23)$$

Where χ is the angle between the two polarizers, β is the angle between the polarizer and the LC directors, as shown in Fig. 2-22. Usually, β=45° and the two polarizers are parallel (χ=0), the normalized light transmittances and reflectance of are simplified to Eqs. 2- 24 and 2- 25:

$$T = \cos^2(\delta_T/2) = \cos^2(2\pi d_T\Delta n/2\lambda) = \cos^2(\pi d_T\Delta n/\lambda) \qquad (2\text{-}24)$$

$$R = \cos^2(\delta_R/2) = \cos^2(2\pi 2d_R\Delta n/2\lambda) = \cos^2(2\pi d_R\Delta n/\lambda) \qquad (2\text{-}25)$$

If we employed $\lambda/4$ retardation films between the polarizer and LC layer, then the Eqs. 2- 24 and 2- 25 should be rewritten to Eqs. 2- 26 and 2- 27:

$$T = \cos^2\left(\frac{\delta_T}{2} + N\cdot\frac{\pi}{4}\right) \qquad (2\text{-}26)$$

$$R = \cos^2\left(\frac{\delta_R}{2} + N\cdot\frac{\pi}{4}\right) \qquad (2\text{-}27)$$

Where N is the total number of the $\lambda/4$ retardation films used in the LCD.

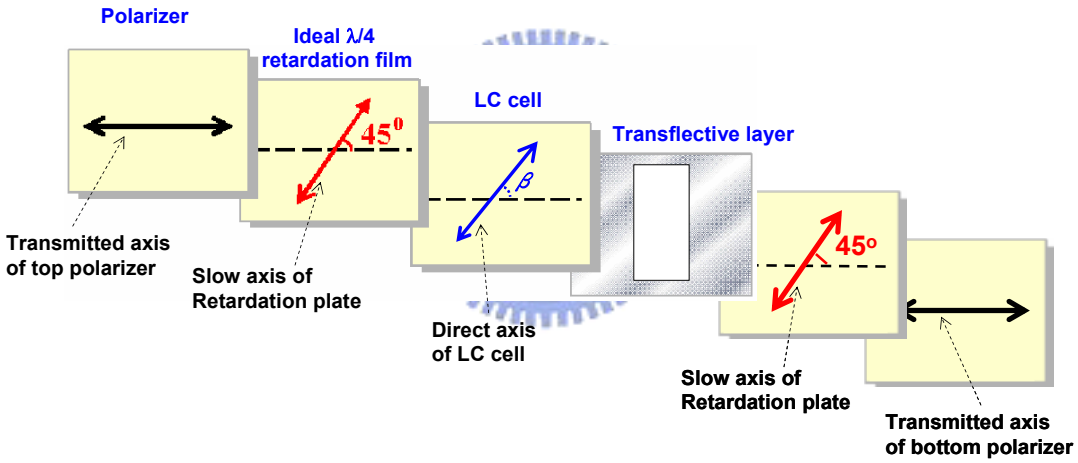

Fig. 2-22. The parameters of a general transflective LCD employing parallel polarizers, two retardation films, and transflective layer.

Based on the phase retardation effect, we can calculate the reflectance and transmittance of transflective LCDs using single or double cell gap structure, as shown in Fig. 2-23. For traditional single cell gap transflective structure, there are two $\lambda/4$ retardation films on the both sides of LC layer, as shown in Fig. 2-24(a), and the liquid crystal fulfills a $\lambda/4$ condition, which is referred to $\delta = \pi/2$. Under the voltage off state, with a pair of crossed polarizer, the transmittance of the LCD equals to only 50% from that shown in Eq. 2- 27, and the reflectance equals to 100%.

Therefore, only half of the light can be used in the transmissive mode. Regarding to the double thickness of LC cell gap in the transmissive region (Fig. 2-24(b)), the phase retardation is referred to $\delta = \pi$. Consequently, the transmittance and reflectance of a double cell gap transflective LCD are 100%.

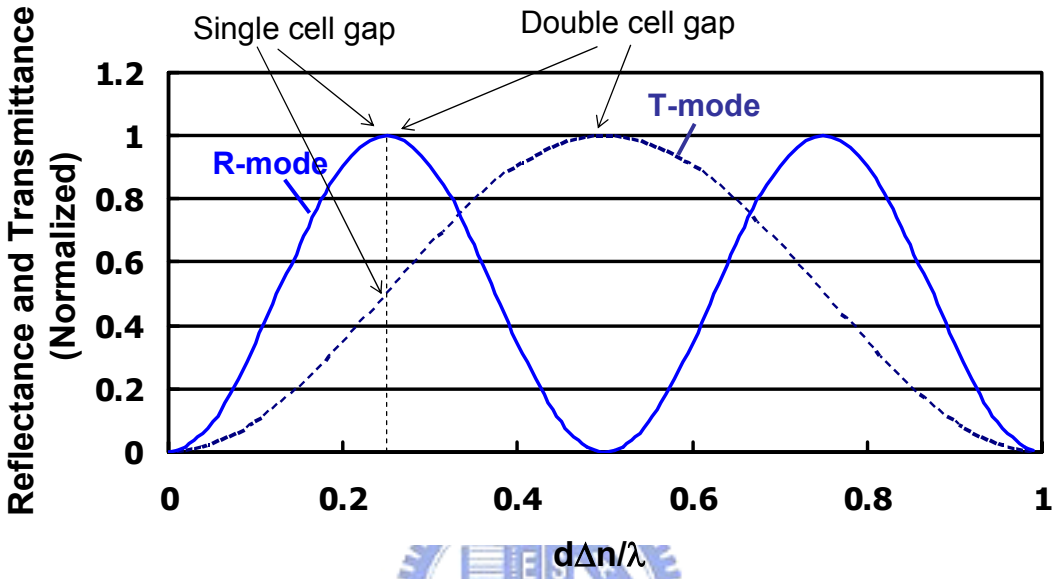

Fig. 2-23. Normalized reflectance and transmittance of transflective LC cell as a function of dΔn/λ.

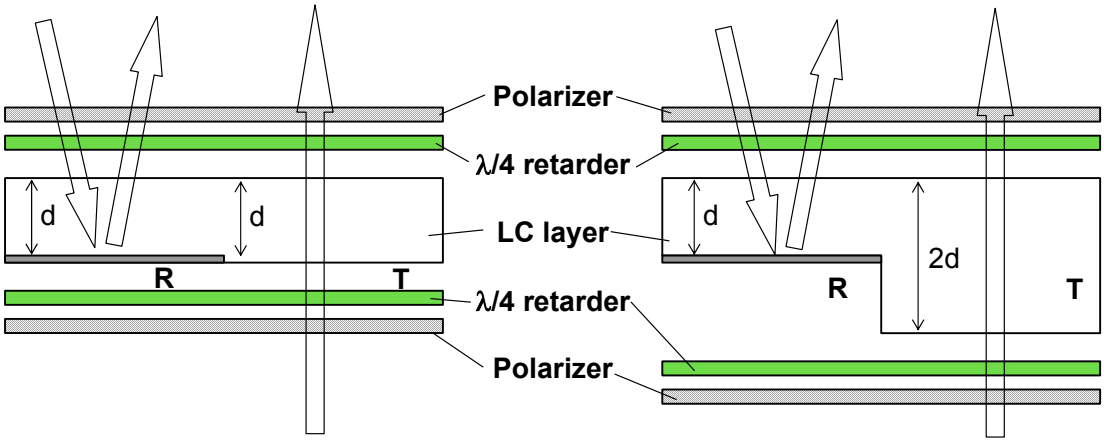

(a) Single cell gap (b) Double cell gap

Fig. 2-24. Schematic plot of transflective LCDs using (a) single cell gap and (b) double cell gap structure[22].

2.3 Summary

The diffractive microoptics and portable LCD technologies have been briefly discussed in this chapter. We presented the fundamental theory and basic design of diffractive microoptical components. To meet both demands for well approximation and fast computing, scalar diffraction theory from Fourier optics is applied in diffractive microoptical component design. Two basic diffractive microoptical components of binary phase prism and Fresnel microlens were introduced, developed, and ingeniously applied to display systems in this thesis work. The mechanism and design rule of these microoptical components were presented to facilitate the basis of this thesis.

The basic working principle and the briefly numerical calculation of various portable LCDs were studied and described. The mixed-mode twisted nematic LCDs and super-twisted nematic LCDs, exhibit high contrast and good color image, and have gradually become the mainstream approach, such as the panel for cellular phone, digital camera, and personal hand-held computer. Contrary, the polymer dispersed liquid crystal (PDLC) and cholesteric LCDs, have the advantage of non-polarizer and wide viewing angle yet with poor contrast and image color, are utilized for smart card, monochrome e-book, etc. Additionally, the numerical formula of a transflective LCD, which provides good legibility under any circumstance, was discussed. In this thesis work, these fundamental working principles are employed for designing the microoptical elements to enhance their image performance.